

NOVEL SHAPE MEMORY ACTUATORS

HISAAKI TOBUSHI, KOUJI MIYAMOTO,
YASUHIKO NISHIMURA, KENTO MITSUI

Aichi Institute of Technology, Department of Mechanical Engineering, Toyota, Japan
e-mail: tobushi@aitech.ac.jp

In order to develop novel shape memory actuators, the torsional deformation of a shape memory alloy (SMA) tape and the actuator models driven by the tape were investigated. The shape memory composite (SMC) belt composed of SMA tapes and a shape memory polymer (SMP) was fabricated, and the three-way bending characteristics were also investigated. The results obtained can be summarized as follows. In the SMA tape subjected to torsion, the martensitic transformation appears along the edge of the tape due to elongation of the edge of the tape and grows to the central part. The fatigue life in both the pulsating torsion and alternating torsion is expressed by a unified relationship of the dissipated work in each cycle. Based on the two-way motion of an opening and closing door model and a solar-powered active blind model driven by two kinds of SMA tape, it is confirmed that the two-way rotary driving actuator with a small and simple mechanism can be developed by using torsion of the SMA-tape. The SMC belt laminated with the SMP tape and SMA tapes was fabricated. The three-way bending movement of the SMC belt was achieved during heating and cooling based on the characteristics of the SMA tapes and the SMP tape. The active SMC actuator with various three-dimensional movements can be developed by applying the three-way properties of the SMC.

Key words: shape memory alloy, shape memory polymer, composite, actuator, two-way, three-way, tape

1. Introduction

In the recent years, intelligent materials having functions of sensing, judging and working have attracted worldwide attention. One of the main materials which have activated the research on the intelligent materials is the shape memory alloy (SMA) (Funakubo, 1987; Otsuka and Wayman, 1998). The main

characteristics of SMA are the shape memory effect (SME) and superelasticity (SE). Thanks to these characteristics, SMAs are used in the driving elements of actuators, heat engines and robots. The SME and SE appear as the result of a martensitic transformation (MT).

The deformation properties of the SME and SE depend strongly on temperature and stress. In a recent study using the torsional deformation of a TiNi SMA tube, twist in the blades of rotor aircraft was investigated in order to improve the flight performance (Mabe *et al.*, 2004, 2007). Because of the adaptable thermal response of SMA elements, thin wires and tapes are widely used in practical applications. In practical applications making use of SMA-tapes, the torsional deformation can be obtained simply by gripping both ends without any mechanical process. If the characteristics of SE are exploited, a high performance of energy storage can be achieved similar to that of a torsion bar. In this way of using torsional characteristics of SMA-tapes, simple and small actuators can be developed. The authors investigated therefore the basic deformation properties of an SMA-tape in torsion (Tobushi *et al.*, 2008, 2009).

The shape memory polymer (SMP) has been also practically used. In SMPs, the elastic modulus and the yield stress are high at temperatures below the glass transition temperature T_g and low at temperatures above T_g . If SMPs are deformed at temperatures above T_g and cooled down to temperatures below T_g by holding the deformed shape constant, the deformed shape is fixed and SMPs can carry large load. If the shape-fixed SMP element is heated up to temperatures above T_g under no load, the original shape is recovered. The shape memory property appears based on the glass transition in which the characteristics of molecular motion vary depending on the variation in temperature. Among the SMPs, the polyurethane SMP has been practically used.

In order to use new and higher functions by combining the excellent qualities of both the SMA and the SMP, the development of a shape memory composite (SMC) with the SMA and SMP is expected (Sterzl *et al.*, 2003; Manzo and Garcia, 2007; Browne *et al.*, 2009; Tobushi *et al.*, 2006, 2010).

In the present paper, in order to develop rotary actuators driven by SMA tapes, the torsional deformation properties of TiNi SMA tapes are investigated. The two-way motions of an opening and closing door model and a solar-powered active blind model driven by SMA tapes are demonstrated. The fabrication and mechanical properties of the SMC belt which shows the three-way bending motion depending on temperature variation are investigated. Based on the three-way characteristics of the SMC belt, the SMC actuators with three-dimensional movement are also discussed.

2. Rotary actuator driven by SMA tape

2.1. Material

The materials used in the experiment were Ti-50.18at%Ni SMA tape with a thickness of $t = 0.25$ mm and a width of $w = 5$ mm. The specimen was a uniform flat tape of length $L = 60$ mm. The gauge length of the specimen was $l = 40$ mm. The transformation temperatures obtained from the DSC test were $M_s = 304$ K, $M_f = 266$ K, $A_s = 319$ K and $A_f = 359$ K.

2.2. Torsional deformation and fatigue properties of SMA tape

2.2.1. Twisted state

The photographs of the twisted SMA tape are shown in Fig. 1 for each angle of twist. The left side shows the fixed end and the right side the twisted end. The crossover point of the upper and lower surfaces of the SMA tape propagates from the twisting end at the angle of twist per unit length $\theta = 39.3$ rad·m⁻¹ (total angle of twist $\phi = \pi/2$) and reaches the central part of the specimen at $\theta = 78.5$ rad·m⁻¹ ($\phi = \pi$). We note that both edges of the tape are elongated by twisting since both ends are axially fixed. Therefore, tensile stress is induced along both edges, and the stress state becomes different from the simple shear and much more complex.

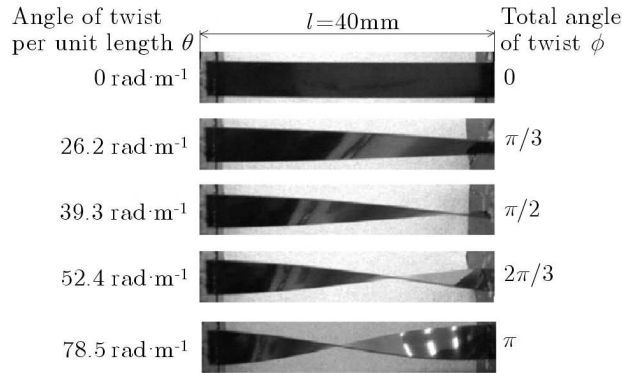


Fig. 1. Photographs of the twisted SMA tape at each angle of twist

2.2.2. Observation of martensitic transformation by thermography

The thermomechanical characteristics of SMA appear due to the MT and the reverse transformation. The exothermic reaction and endothermic reaction

occur based on the MT and the reverse transformation, respectively. In the DSC test, the transformation temperatures are determined by measuring the heat change owing to these reactions. In the case of SE due to the stress-induced MT, temperature increases or decreases in the loading and unloading processes, respectively. The initiation and growth processes of the MT can be therefore analyzed by measuring temperature on the surface of the material. The infrared thermography to measure the temperature distribution on the whole surface of the material can be applied to this objective. The MT behavior of SMA can be analyzed by the thermography (Pieczyńska *et al.*, 2006).

The temperature distribution on the surface of the SMA tape at each angle of twist during the torsional deformation obtained by the infrared thermography is shown in Fig. 2. In Fig. 2, the upper side in each case shows the twisting part and the lower side shows the fixed part. The maximum temperature T_{max} on the surface of the specimen appears along the edge of the tape, and the exothermic MT occurs in this part and grows toward the central part of the specimen. The temperature rise along the edge of the tape starts at the angle of twist per unit length $\theta = 26.2 \text{ rad}\cdot\text{m}^{-1}$. This angle of twist per unit length corresponds to the tensile strain at the edge of the tape of 0.3% and coincides with the MT starting condition. The maximum temperature of the specimen occurs along the edge of the tape and the high temperature region propagates toward the central part with an increase in the angle of twist. Therefore, the MT grows preferentially based on the elongation along the edge of the tape.

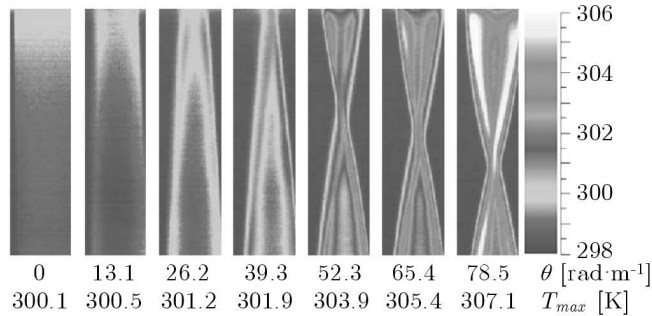


Fig. 2. Thermograms showing temperature distribution on the surface of the SMA tape appeared due to the phase transformation under torsion

2.2.3. Torsional deformation

The relationships between the torque M and angle of twist per unit length θ obtained by the pulsating torsion test and the alternating torsion test for the maximum angle $\theta_m = 78.5 \text{ rad}\cdot\text{m}^{-1}$ are shown in Figs. 3a and 3b, respectively.

In the case of the pulsating torsion, the curve between M and θ is expressed almost by a straight line in the first loading process. In the unloading process, the initial slope of the curve is steep, and thereafter becomes to be the plateau stage. In the reloading process, the initial curve is almost parallel to the first loading curve, and thereafter the slope of the curve becomes steep. In the case of the alternating torsion, the twisting in the reverse direction to the first twisting direction was carried out. The reverse loading and unloading curves are almost similar to the first loading and unloading curves except for the early stage. That is, the first and reloading curves are closely symmetric with respect to the origin. In the reloading process, the initial slope of the unloading curve is steep and the plateau stage appears thereafter. The point at the end of the reloading curve almost coincides with the point at which the first unloading started, showing the return-point memory in the pulsating and alternating torsion.

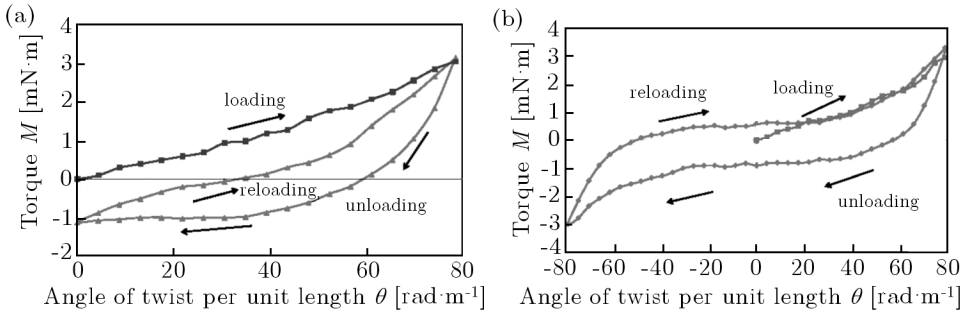


Fig. 3. Relationship between the torque M and angle of twist per unit length θ obtained by the pulsating and alternating torsion tests for the maximum angle $\theta_m = 78.5 \text{ rad}\cdot\text{m}^{-1}$

The area surrounded by the hysteresis loop of the torque-angle curve of twist shown in Fig. 3 expresses the dissipated work per unit length W_d . The dissipated work W_d increases in proportion to the maximum angle of twist θ_m . The value of W_d in the alternating torsion is larger than that in the pulsating torsion by 3.5 times. W_d is very small if θ_m is smaller than a certain value in both alternating and pulsating torsion.

2.2.4. Torsional fatigue properties

The relations between the maximum angle of twist per unit length θ_m and the number of cycles to failure N_f obtained from the torsion fatigue test are shown in Fig. 4. The number of cycles to failure N_f decreases with an increase in the maximum angle of twist per unit length θ_m . This relation is

approximated by a straight line on the logarithmic graph. The fatigue life curve seems therefore to be expressible in an equation similar to that for TiNi SMA wires under bending. This can be seen in Eq. (2.1)

$$\theta_m N_f^\beta = \alpha \tag{2.1}$$

where α and β represent θ_m in $N_f = 1$ and the slope of the $\log \theta_m - \log N_f$ curve, respectively. The calculated results obtained from Eq. (2.1) for $\beta = 0.1$, $\alpha = 265 \text{ rad}\cdot\text{m}^{-1}$ in pulsating torsion and for $\beta = 0.13$, $\alpha = 310 \text{ rad}\cdot\text{m}^{-1}$ in alternating torsion are shown by the solid lines in Fig. 4. As can be seen, the fatigue life curves are well matched by the solid calculation lines. Comparing the fatigue life of alternating torsion and pulsating torsion, the number of cycles to failure N_f for alternating torsion is smaller than that for pulsating torsion by 1/5.

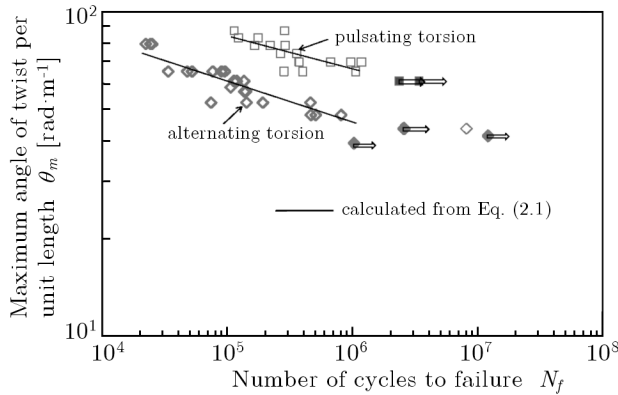


Fig. 4. Relationship between the maximum angle of twist per unit length and the number of cycles to failure

The relationship between the dissipated work W_d and the number of cycles to failure N_f is shown in Fig. 5. The relationships for the pulsating torsion and the alternating torsion are located almost on the same line. The fatigue life in both the pulsating torsion and the alternating torsion is therefore expressed by a unified relationship. The relationship between N_f and W_d can be expressed by a power function in Eq. (2.2)

$$W_d N_f^\lambda = \mu \tag{2.2}$$

where μ and λ represent W_d at $N_f = 1$ and the slope of the $\log W_d - \log N_f$ curve, respectively. The calculated result by Eq. (2.2) for $\lambda = 0.382$ and $\mu = 9 \text{ J/m}$ is shown by the solid line in Fig. 5. As can be seen, the overall inclinations are approximated by the solid line. The dissipated work corresponding

to the fatigue limit may exist at 0.04-0.05 J/m. If the dissipated work in each cycle is smaller than 0.04-0.05 J/m, the fatigue damage is slight, resulting in long fatigue life.

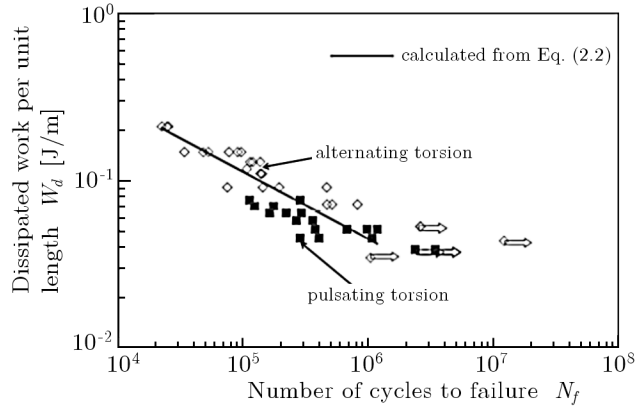


Fig. 5. Relationship between dissipated work per unit length and number of cycles to failure

2.3. Two-way opening and closing door model

Photographs of the rotary movement of an opening and closing door model using an SMA tape which shows the SME and an SEA tape which shows SE at RT under heating and cooling are shown in Fig. 6. The SMA tape is the same as the specimen used in the torsion test. The SEA tape with a thickness of $t = 0.25$ mm and a width of $w = 2.5$ mm was a TiNi SEA tape which was heat-treated to memorize a flat plane. In the initial state at RT, the SEA tape was mounted to be in a flat plane and the SMA tape was mounted at the total angle of twist $\phi = \pi/2$. The SMA tape was heated by joule heat through electric current. As can be seen in Fig. 6, the door is closed in the initial state, since torque of SEA tape M_{SEA} is larger than that of the SMA tape M_{SMA} . Since the recovery torque appears by heating the SMA tape and the relation of the torque changes into $M_{SMA} > M_{SEA}$, the SMA tape recovers the flat plane and, therefore, the door is opened. When the SMA tape is cooled thereafter, the relation of torque varies again into $M_{SMA} < M_{SEA}$. Therefore, the SEA tape recovers the flat plane, resulting in closing the door. Thus, if two kinds of SMA tapes which show the SME and SE are used, a two-way rotary driving element with a small and simple mechanism can be developed.

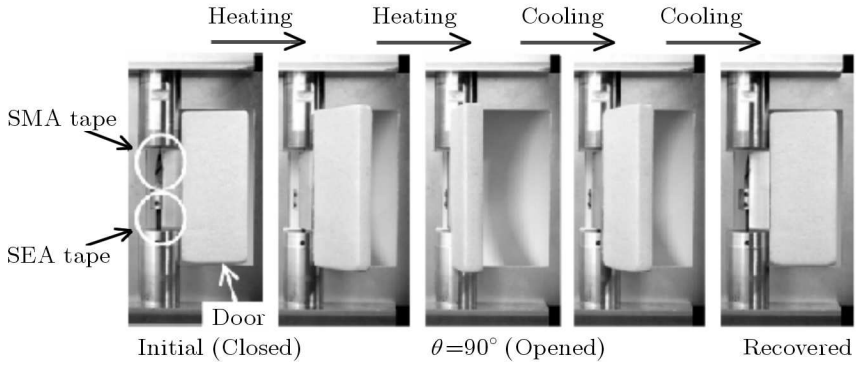


Fig. 6. Photographs of two-way rotary movement of a door driven by the SMA tape and SEA tape during heating and cooling

2.4. Solar-powered active blind model

A new rotary actuator model in which the axes of an SMA tape and an SEA tape are arranged in parallel is demonstrated.

The structure of a two-way actuator for opening and closing a blind driven by the SMA tape and SEA tape through sunlight, the photograph of the solar-powered active blind and the photographs of two-way motion of the actuator are shown in Figs. 7, 8 and 9, respectively. Both the SMA tape and the SEA tape were the same as those used in the door model. In the initial state, the SEA tape was mounted to be in a flat plane and the SMA tape was mounted at the total angle of twist $\phi = \pi/2$.

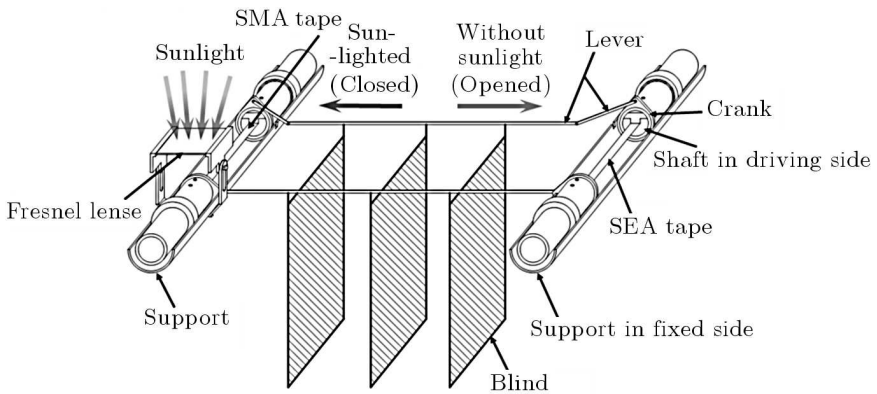


Fig. 7. Structure of the solar-powered active blind

The SMA tape was heated by sunlight through a Fresnel lens. Since the recovery torque appears in the SMA tape by heating the tape, the blind is

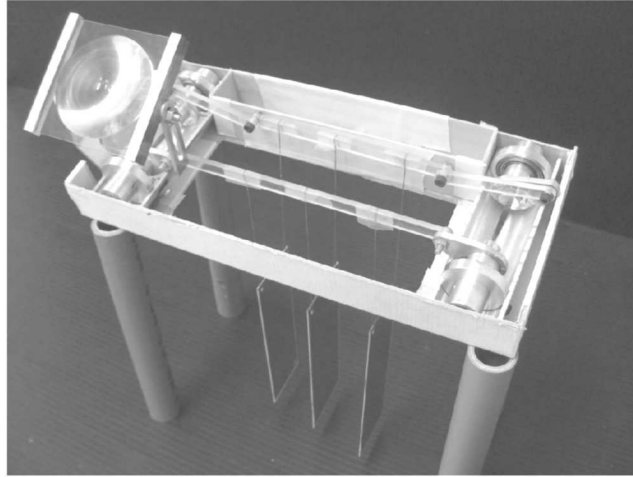


Fig. 8. Photograph of the solar-powered active blind

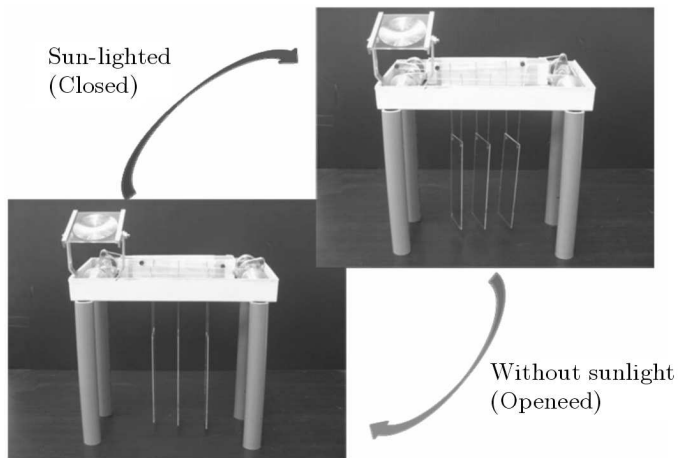


Fig. 9. Photographs of two-way motion for the opening and closing of the blind driven by sunlight through the SMA tape and SEA tape

closed through a crank and a lever. When the sunlight is shut out, the SMA tape is cooled and the SEA tape recovers the flat plane, resulting in the opening of the blind. Thus, if two kinds of SMA tapes which show the SME and SE are used, the two-way rotary actuator driven by sunlight can be developed.

3. Three-way active shape memory composite actuator

3.1. Material

With respect to the SMA, two kinds of polycrystalline SMA tapes showing the SME and SE at room temperature were used. The SMA tape showing the SME was a TiNi alloy tape with a width of 5 mm and a thickness of 0.3 mm produced by Furukawa Techno Materials Co. The SEA tape showing the SE was a TiNi alloy tape with a width of 2.5 mm and a thickness of 0.25 mm produced by Yoshimi Inc. In the shape memory processing, each SMA tape was set along the inside of a fixing ring with an inner diameter of 16 mm and was heat-treated to memorize the round shape with an outside diameter of 16 mm. The temperatures A_s and A_f of the SMA tape were 324 K and 342 K, and these of the SEA tape were 287 K and 309 K, respectively. The R-phase transformation start and finish temperatures R_s and R_f of the SMA tape were 322 K and 309 K, respectively.

With respect to the SMP, a polyurethane SMP sheet (MM6520) produced by SMP Technologies Inc. was used. The thickness was 0.25 mm and the glass transition temperature T_g was 338 K.

3.2. Structure of SMC belt

The SMC belt with a length of 60 mm, a width of 10 mm and a thickness of 1.03 mm was fabricated by using two kinds of SMA tapes and three SMP tapes. In the fabricated SMC belt, the SMP tapes were used as a matrix and the SMA tapes as a fiber. The length of the SMA tape and the SEA tape was 50 mm. Two kinds of SMA tapes were located in the central part of the SMC belt. The structure of the SMC belt is shown in Fig. 10.

3.3. Fabrication of SMC belt

At first, two incisions were given to one SMP tape and two kinds of SMA tapes (SMA tape and SEA tape) were passed through these incisions. In this process, the SMA tape and SEA tape were arranged facing in the opposite directions for the memorized round shape as shown in Fig. 11. The SMP tape passed through two kinds of SMA tapes was sandwiched between two SMP tapes from the upper and lower sides. The combined material was set in the mold for fabricating the SMC belt. The upper and lower molds were fastened through the bolts by a compressive stress of 7.46 MPa. The mold was held in the furnace at 448 K for 60 min followed by cooling in air. The SMC belt without bubbles and gaps among the materials could be fabricated under these

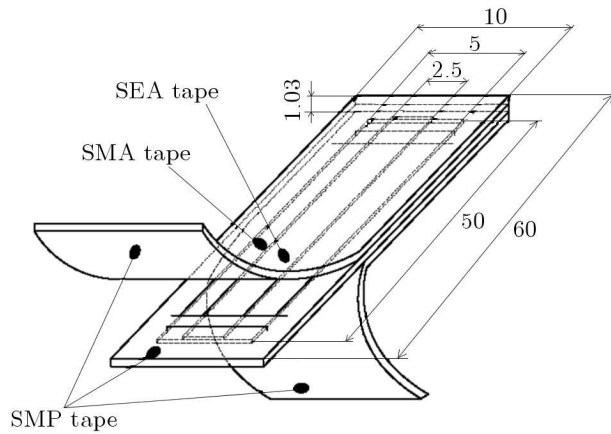


Fig. 10. Structure of the SMC belt composed of the SMA, SEA and SMP tape

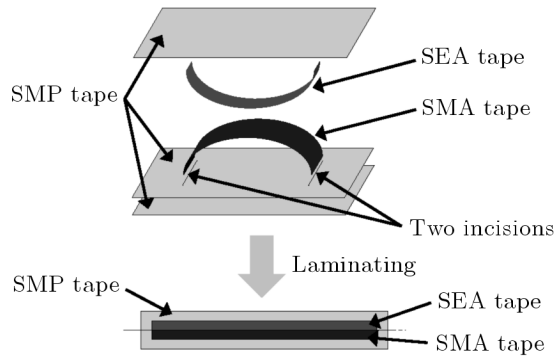


Fig. 11. Arrangements of the SMA, SEA and SMP tapes to laminate the SMC belt

conditions. In order to protect the projection of the edge by the recovery force of the SMA tapes, both edges of the SMA tapes were connected by a thin steel clamp.

3.4. Three-way actuation

The photographs of the three-way bending motion of the fabricated SMC belt during heating and cooling are shown in Fig. 12. The heating and cooling were carried out between 293 K and 365 K. In Fig. 12, the symbols $A_{s,SEA}$, $A_{f,SEA}$, $A_{s,SMA}$, $A_{f,SMA}$ and T_g represent the reverse-transformation start and finish temperatures of the SEA tape and the SMA tape and the glass transition temperature of the SMP tape, respectively. At 293 K ①, the force induced in the SEA tape is high, and therefore the SMC belt bends in the

direction of the shape-memorized round shape of the SEA tape. If the SMC belt is heated ①-②, the SMP becomes soft and the SMC belt bends further in the same direction at temperatures around T_g ②. If the SMC belt is heated up above T_g ①-③, the SMP becomes easier to deform and the recovery force in the SMA tape increases at temperatures above $A_{f,SMA}$ (Lin *et al.*, 1995), and therefore the SMC belt bends in the direction of the shape-memorized round shape of the SMA tape ③. If the SMC belt is cooled thereafter ③-④, the recovery force in the SMA tape decreases and the recovery force in the SEA tape becomes higher. Therefore, the SMC belt bends again to its original shape ④.

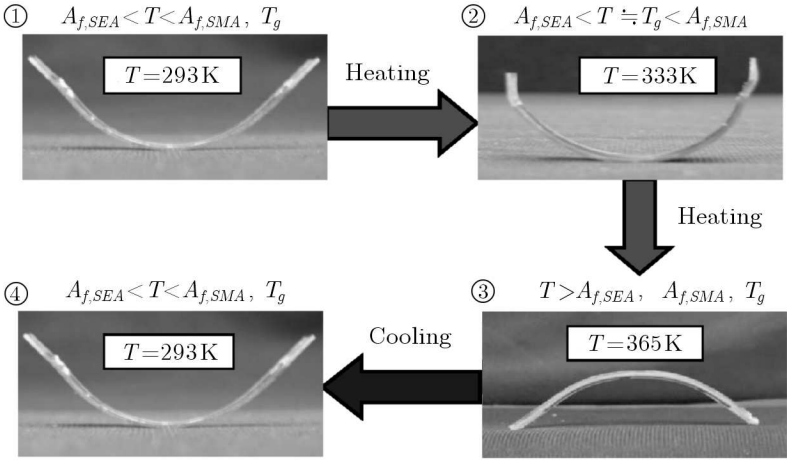


Fig. 12. Photograph of the three-way bending deformation of the SMC belt during heating and cooling

3.5. Movement in three-point bending

The three-way movement was measured by the three-point bending test. At first, the initial bent-form SMC belt was set on the supports of the three-point bending test machine. After setting the SMC belt, the point of the punch contacted slightly the center of the SMC belt. Keeping the slight contact condition with the contact load lower than 0.1N, the SMC belt was heated and cooled, and the displacement at the center of the SEC belt was measured.

The relationship between the displacement and temperature obtained by the three-point bending test is shown in Fig. 13. $R_{s,SMA}$ and $R_{f,SMA}$ denote the *R*-phase transformation start and finish temperatures of the SMA tape, respectively. The symbols ①-④ correspond to the deformed states ①-④ shown

in Fig. 12. It should be noticed that if the deflection of the SMC belt increases, the center of the SMC belt moves downward and the displacement decreases to the negative side. In the heating process ①-②, the deflection of the SMC belt increases, since the SMP exists in the glass transition region ② and the SMP becomes soft. In the heating process ②-③, the deflection of the SMC belt decreases, since the internal bending moment of the SMA tape increases at temperatures around $A_{f,SMA}$ due to the reverse transformation of the SMA tape. In the cooling process ③-④, the deflection of the SMC belt increases gradually with a decrease in temperature since the internal bending moment of the SMA tape decreases due to the R -phase transformation and, therefore, the internal bending moment of the SEA tape becomes higher than that of other elements.

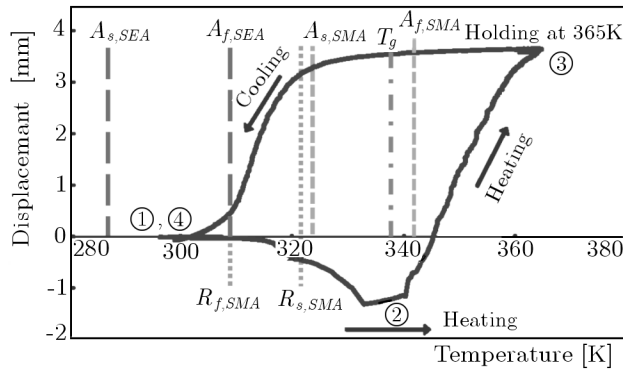


Fig. 13. Relationship between the displacement and temperature of the SMC belt obtained by the three-point bending test

3.6. Recovery force in three-point bending

In the three-point bending test with heating and cooling for the recovery force, the center of the SMC belt was put in the punch, and the position was held constant. Keeping the position of the center and two supports constant, the SMC belt was heated and cooled.

The relationship between the recovery force and temperature obtained by the three-point bending test for the SMC belt is shown in Fig. 14. The behavior of the recovery force is different between the heating process and cooling process, and the curve describes a large hysteresis loop. In the heating process, the recovery force of the SMC belt decreases at temperatures around T_g of the SMP ②. The recovery force starts to increase at temperatures around $A_{f,SMA}$ of the SMA tape. Since the recovery force of the SMA tape becomes stronger than that of the SEA tape at temperatures around $A_{f,SMA}$, the recovery

force of the SMC belt appears. In the cooling process, the recovery force of the SMC belt decreases gradually. The recovery force of the SMA tape decreases due to the R-phase transformation at temperatures between $R_{s,SMA}$ and $R_{f,SMA}$ (Lin *et al.*, 1995), and the recovery force of the SMC belt decreases correspondingly.

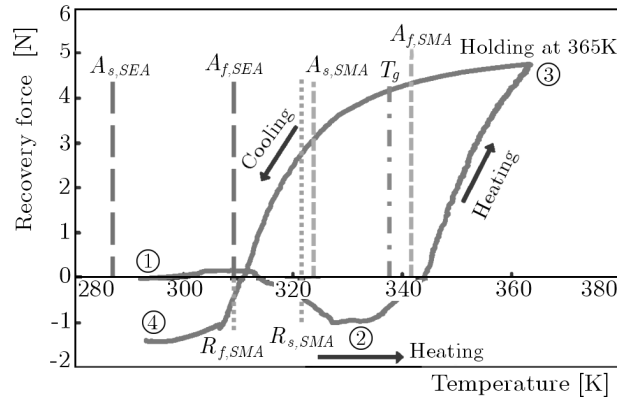


Fig. 14. Relationship between the recovery force and temperature of the SMC belt obtained by the three-point bending test

3.7. SMC actuator with three-dimensional movement

The three-way bending movement in a plane was obtained by the fabricated SMC belt. In the SMC belt, the SMA tape and SEA tape were arranged in the same direction and laminated with the SMP tape. If both tapes are arranged in different directions and sandwiched between SMP sheets, the SMC sheet moves not only in a plane but also moves in various planes during heating and cooling. Therefore, the SMC actuator with three-dimensional movement can be developed by applying the three-way properties of SMC with various combinations of the SMA, SEA and SMP elements. The three-dimensional movement properties of the SMC actuator depend on the memorized shapes, configurations, volume fractions and phase transformation temperatures of each element.

4. Conclusions

In order to develop the rotary driving element with SMA tape, the torsional deformation properties and actuator models driven by a TiNi SMA tape were investigated. The SMC belt composed of two kinds of SMAs and SMP was

fabricated, and the three-way movement and recovery force in bending were also investigated. The results obtained can be summarized as follows.

- In the SMA tape subjected to torsion, the MT appears along the edge of the tape due to elongation of the edge of the tape and grows to the central part. The fatigue life in both the pulsating torsion and the alternating torsion is expressed by the unified relationship of the dissipated work in each cycle.
- Based on the two-way motion of the opening and closing door model and the solar-powered active blind model driven by two kinds of SMA tape, it is confirmed that the two-way rotary driving actuator with a small and simple mechanism can be developed by using torsion of the SMA tapes.
- The SMC belt was fabricated by laminating the SMP tape and two kinds of SMA tapes arranged facing in the opposite directions for the shape-memorized round shape. The three-way bending movement of SMC belt was achieved during heating and cooling based on the characteristics of the SMA tapes and the SMP tape. The active SMC actuator with various three-dimensional movements can be developed by applying the three-way properties of the SMC.

Acknowledgements

The experimental work for this study was carried out with the assistance of students in Aichi Institute of Technology, to whom the authors wish to express their gratitude. The authors are also grateful to the administrators of Scientific Research (C) (General) in Grant-in-Aid for Scientific Research by the Japan Society for the Promotion of Science and The Naito Research Grant for financial support.

References

1. BROWNE A.L. ET AL., 2009, Programmable shims for manufacturing and assembly lines, U.S. Patent, 7538472 B2, 1-24
2. FUNAKUBO H. EDIT., 1987, *Shape Memory Alloys*, Gordon and Breach Science, New York
3. LIN P.H., TOBUSHI H., TANAKA K., LEXCELLENT C., IKAI A., 1995, Recovery stress of TiNi shape memory alloy under constant strain, *Arch. Mech.*, **47**, 2, 281-293

4. MABE J.H., CALKINS F.T., RUGGERI R.T., 2007, Full-scale flight tests of aircraft morphing structures using SMA actuators, *Proc. of SPIE*, **6525**-65251C, 1-12
5. MABE J.H., RUGGERI R.T., ROSENZWEIG E., YU C.J., 2004, Nitinol performance characterization and rotary actuator design, *Proc. of SPIE*, **5388**, 95-109
6. MANZO J.E., GARCIA E., 2007, Active rigidity smart joint for a bat-wing micro air vehicle, *Proc. of ASME IMECE*, 231-241
7. OTSUKA K., WAYMAN C.M., 1998, *Shape Memory Materials*, Cambridge University Press, Cambridge
8. PIECZYSKA E.A., GADAJ S.P., NOWACKI W.K., TOBUSHI H., 2006, Phase-transformation fronts evolution for stress- and strain-controlled tension tests in TiNi shape memory alloy, *Exp. Mech.*, **46**, 531-542
9. STERZL T., WINZEK B., MENNICKEN M., NAGELSDIEK R., KEUL H., HOCKER H., QUANDT E., 2003, Bistable shape memory thin film actuators, *Proc. of SPIE*, **5053**, 101-109
10. TOBUSHI H., HAYASHI S., HOSHIO K., MAKINO Y., MIWA N., 2006, Bending actuation characteristics of shape memory composite with SMA and SMP, *J. Intell. Mater. Syst. Struct.*, **17**, 1075-1081
11. TOBUSHI H., HAYASHI S., SUGIMOTO Y., DATE K., 2010, Fabrication and two-way deformation of shape memory composite with SMA and SMP, *Mater. Sci. Forum*, **638-642**, 2189-2194
12. TOBUSHI H., PIECZYSKA E.A., NOWACKI W.K., SAKURAGI T., SUGIMOTO Y., 2009, Torsional deformation and rotary driving characteristics of SMA thin strip, *Arch. Mech.*, **61**, 3-4, 241-257
13. TOBUSHI H., SAKURAGI T., SUGIMOTO Y., 2008, Deformation and rotary driving characteristics of a shape-memory alloy thin strip element, *Mater. Trans.*, **49**, 1, 151-157

Nowe aktuatory z elementami z pamięcią kształtu

Streszczenie

W pracy zajęto się aktuatorami nowego typu, w których zastosowano stop z pamięcią kształtu (SMA) w postaci skręcającej się taśmy SMA wywołującej ruch aktuatora. Opracowano kompozytowy pas (SMC) z taśm SMA oraz polimeru wykazującego efekt pamięci kształtu (SMP) oraz zbadano charakterystyki takiego kompozytu przy zginaniu trójosiowym. Rezultaty badań pokazały, że taśma SMA poddana skręcaniu doznaje przemiany martenzytycznej wzdłuż krawędzi z powodu jej wydłużania,

która stopniowo przechodzi do środkowej części taśmy. Problem wytrzymałości zmęczeniowej taśmy obciążonej jednokierunkowym i naprzemiennym skręcaniem opisano ujednoczonym wyrażeniem określającym pracę dyssypacji na każdy cykl obciążenia. Zbadano model aktuatora dwustronnego działania do otwierania i zamykania drzwi oraz do sterowania przesłony zasilanej energią słoneczną. Potwierdzono skuteczność torsyjnego aktuatora SMA przy utrzymaniu prostoty konstrukcji takiego mechanizmu. Przeanalizowano przestrzenny ruch kompozytowego pasa SMC indukowanego ogrzewaniem i chłodzeniem w zależności od charakterystyk taśm SMA i SMP. Pokazano, że dzięki właściwościom kompozytu SMC różnych w trzech kierunkach, uzyskanie zdolności ruchowej aktuatora w przestrzeni (3D) jest możliwe.

Manuscript received January 14, 2011; accepted for print March 3, 2011